

# Optimal Operation of Islanded AC/DC Hybrid Microgrids

Arif Ahmed\*, Evangelos Pompodakis†, and Tobias Massier‡

\*‡TUMCREATE, 1 CREATE Way, #10-02 CREATE Tower, Singapore 138602

†Electrical & Computer Engineering, Aristotle University of Thessaloniki, Thessaloniki 54124, Greece

Email: \*arif.ahmed@tum-create.edu.sg, †bobodakis@hotmail.com, ‡tobias.massier@tum-create.edu.sg

**Abstract**—This manuscript presents a single-phase power flow approach and an optimal power flow formulation for islanded AC/DC hybrid microgrids. Conventional operation of hybrid microgrids with fixed droop gains may yield undesirable operation, such as violation of frequency and voltage limits, or increased cost of operation. The proposed optimal power flow formulation mitigates these issues. Optimal power flow is formulated as a constrained multi-objective nonlinear cost minimization problem. A year-long case study was carried out for a 12-bus islanded AC/DC hybrid microgrid using the single-phase power flow approach in conventional and optimal power flow formulation. Simulation results highlight the effectiveness of the proposed approach.

**Index Terms**—AC/DC Hybrid Microgrids, Optimal operation, AC/DC Power Flow, Optimal Power Flow

## I. INTRODUCTION

Microgrids gained widespread popularity and are expected to be an enabling technology in pursuit of a cleaner energy future. The proliferation of distributed generators (DGs) such as solar photovoltaics (PV), battery storage systems or fuel cells – which are dominantly DC energy sources – are important components of the modern microgrid. Therefore, the need for hybrid microgrids, which interlink both AC and DC networks accommodating various types of loads and generators are becoming more and more important, and are expected to play an essential role in the future. In addition, technologies like electric vehicles are becoming dominant and expected to grow, resulting in an increase in the need for more efficient microgrids. Amongst the advantages of hybrid microgrids are various types of generation and load integration, power sharing, improved voltage profiles and network capacity [1].

Numerous studies pertaining to power flow and control strategy of AC/DC hybrid microgrids have emerged recently [2]–[6]. In [2], the authors presented an improved droop control scheme for the interlinking converter in an AC/DC hybrid microgrid to facilitate power transfer between the overloaded and underloaded subgrids. Authors in [3] presented a power flow approach for unbalanced AC/DC hybrid microgrids based on the implicit  $Z_{BUS}$  method having fast convergence and ease of implementation. In [4], authors presented a sequence-component based modified Newton-Raphson power flow algorithm for hybrid microgrids. A single-phase power flow approach for hybrid microgrids was presented in [5], where the power flow was solved by formulating an unconstrained minimization problem and utilizing the trust region method. Similarly, in [6], the authors proposed a single-phase load flow approach for hybrid microgrids by formulating a minimization problem based on the generalized reduced gradient method.

There is a lack of studies related to optimal power flow of AC/DC hybrid microgrids over longer time horizons in the literature and a fast convergent and easy to implement single-phase power flow algorithm for hybrid microgrids has not been proposed and investigated yet, either. In this paper, we present a fast-convergent droop-based power flow algorithm for islanded AC/DC hybrid grids based on the implicit  $Z_{BUS}$  power flow algorithm. The algorithm incorporates the droop equations of the DGs, therefore the traditional slack bus assumptions are not utilized as they would lead to inaccurate results. The power flow solution also calculates the system frequency unlike conventional power flow approaches. The optimal power flow formulation is formulated as a constrained multi-objective nonlinear cost minimization problem. A year-long simulation study was carried out for a 12-bus islanded AC/DC hybrid microgrid. The adversities arising from conventional operation of AC/DC hybrid microgrid with fixed droops were identified using the proposed power flow approach.

Section II presents power flow modelling for droop-controlled islanded AC/DC hybrid microgrids. Section III presents the optimal power flow formulation. A year-long simulation case study is undertaken in Section IV, the results are discussed in Section V. The manuscript is concluded in Section VI.

## II. AC/DC HYBRID MICROGRID POWER FLOW MODELLING

### A. Power Flow in Islanded AC Subgrid

Unlike conventional AC grids, in islanded AC subgrids, there is not a sufficiently large DG to take up the role of a slack bus. In conventional power flow, the slack bus is specified with a fixed voltage magnitude and angle, while the active and reactive power injection by the slack bus are unknown and calculated via the power flow solution. However, in islanded AC subgrids with droop-controlled DGs, the voltage magnitude and angle, the active and reactive power injections by the DGs are all unknowns and only the droop values of the DGs are specified. The relationship between generated power ( $P_{G_i}^{ac}$ ,  $Q_{G_i}^{ac}$ ), voltage frequency ( $f$ ), voltage magnitude ( $|V_i^{ac}|$ ), and droop gains ( $K_{P_i}^{ac}$ ,  $K_{Q_i}^{ac}$ ) for  $DG_i^{ac}$  connected at bus  $i$  is given as [3], [4], [7], [8]:

$$f = f_0 - K_{P_i}^{ac} P_{G_i}^{ac} \quad (1)$$

$$|V_i^{ac}| = |V_0^{ac}| - K_{Q_i}^{ac} Q_{G_i}^{ac} \quad (2)$$

In Eq. (1) and (2),  $f_0$  and  $|V_0^{ac}|$  are the no-load voltage's frequency and magnitude, respectively.  $K_{P_i}^{ac}$  and  $K_{Q_i}^{ac}$  are given as [3], [4], [7], [8]:

$$K_{P_i}^{ac} = (f_{max_i} - f_{min_i}) / P_{rated_i} \quad (3)$$

$$K_{Q_i}^{ac} = (|V_{max_i}^{ac}| - |V_{min_i}^{ac}|) / Q_{rated_i} \quad (4)$$

In Eq. (3) and (4),  $f_{max_i}$  is the maximum frequency,  $f_{min_i}$  is the minimum frequency,  $P_{rated_i}$  is the rated active power generation,  $|V_{max_i}^{ac}|$  is the maximum voltage magnitude,  $|V_{min_i}^{ac}|$  is the minimum voltage magnitude, and  $Q_{rated_i}$  is the rated reactive power generation of  $DG_i^{ac}$ .

In the proposed power flow approach, to solve for the AC subgrid, a virtual bus connected to any arbitrary bus in the AC subgrid through a freely selected impedance ( $Z_{vir}$ ) is introduced. The modification becomes necessary as implicit  $Z_{BUS}$  is conventionally used in networks with a slack bus. The virtual bus acts as a conventional slack bus in the network. However, after every iteration, the real power contributed by the slack bus is transferred over to the DGs in the AC subgrid based on their droop gains, and the voltage of the virtual bus is equalized to its adjacent connecting bus. As such, as the power flow algorithm converges, the virtual bus obtains a voltage equal to its adjacent connecting bus and, therefore, contributes no active or reactive power into the network, while the DGs have taken over all the required active and reactive generation of the network [3], [7]. Consequently, the virtual bus has no physical significance in the network.

As a first step to the power flow in the AC subgrid, the current injection at the buses are considered for an  $n$ -bus network having introduced the arbitrarily chosen virtual AC bus as:

$$\begin{bmatrix} I_{vir}^{ac} \\ I_1^{ac} \\ \vdots \\ I_n^{ac} \end{bmatrix} = \begin{bmatrix} Y_{(vir)(vir)} & Y_{(vir)1} & \cdots & Y_{(vir)n} \\ Y_{1(vir)} & Y_{11} & \cdots & Y_{1n} \\ \vdots & \vdots & \ddots & \vdots \\ Y_{n(vir)} & Y_{n1} & \cdots & Y_{nn} \end{bmatrix} \begin{bmatrix} V_{vir}^{ac} \\ V_1^{ac} \\ \vdots \\ V_n^{ac} \end{bmatrix} \quad (5)$$

Subsequently, we remove the current and admittances from the first row of Eq. (5) resulting in the following equation:

$$\mathbf{I}^{ac} = [\mathbf{Y}_A \quad \mathbf{Y}_B] \begin{bmatrix} V_{vir}^{ac} \\ \mathbf{V}^{ac} \end{bmatrix} \quad (6)$$

In Eq. (6),  $\mathbf{I}^{ac}$  is the current injection vector of the original  $n$ -bus network of dimension  $n \times 1$ ,  $\mathbf{Y}_A$  is a vector of dimension  $n \times 1$ ,  $\mathbf{Y}_B$  is a matrix of dimension  $n \times n$ , and  $\mathbf{V}^{ac}$  is the bus voltage vector with dimension  $n \times 1$ .

Finally, Eq. (6) is rearranged to obtain the iterative power flow solution, as presented in Eq. (7), where  $k$  denotes the iteration number. It should be noted that none of the elements on the right hand side of Eq. (7) are constant. Instead, they are updated in every iteration.

$$(\mathbf{V}^{ac})^{k+1} = \mathbf{Y}_B^{-1} (\mathbf{I}^{ac} - \mathbf{Y}_A \cdot V_{vir}^{ac})^k \quad (7)$$

As a droop controlled network, the admittance matrix components are updated based on the calculated system frequency, the current injections are calculated based on the DG and load power injections, and the voltage of the virtual bus is updated in every iteration as mentioned before.

To perform a power flow, the voltages are initialized with a flat start and the relevant components of the system admittance matrix are calculated based on the no-load system frequency. Then the initial current injections are calculated. DGs yield no injection initially at no-load frequency (refer Eq. (1)), while the current injections at PQ buses are calculated based on the flat start voltage. Eq. (7) is then executed to obtain new voltage

estimates. The power flowing through the virtual bus is then calculated, and subsequently, the system frequency is calculated as:

$$f^{k+1} = f^k + P_{vir}^{ac} / \sum_{i \in \mathcal{G}_{ac}} \frac{1}{K_{P_i}^{ac}} \quad (8)$$

In Eq. (8),  $\mathcal{G}_{ac}$  refers to the set of all DGs in the AC subgrid. Based on the calculated frequency and voltage, the active and reactive power injections by the DGs are then calculated based on their droop gains (refer Eq. (1) and (2)). Then the virtual bus voltage is equalized to its adjacent connecting bus and the process is repeated until a specified error tolerance is met to finally obtain a power flow solution for the AC subgrid.

### B. Power Flow in Islanded DC Subgrid

Similar to islanded AC subgrids, DGs in islanded DC subgrids also operate in droop-controlled mode due to the lack of a slack bus. A DG in a DC subgrid may operate in a  $I - V$  or  $P - V$  droop-controlled mode. These relationships for a  $DG_i^{dc}$  in a DC microgrid connected to bus  $i$  are given as:

$$V_i^{dc} = V_0^{dc} - K_{I_i}^{dc} I_{G_i}^{dc} \quad (9)$$

$$V_i^{dc} = V_0^{dc} - K_{P_i}^{dc} P_{G_i}^{dc} \quad (10)$$

In Eq. (9) and (10),  $V_i^{dc}$  is the output voltage,  $V_0^{dc}$  is the no-load voltage,  $K_{I_i}^{dc}$  is the  $I - V$  droop gain,  $K_{P_i}^{dc}$  is the  $P - V$  droop gain,  $I_{G_i}^{dc}$  is the generated DG current, and  $P_{G_i}^{dc}$  is the generated DG active power of  $DG_i^{dc}$  connected at bus  $i$ . Similar to Eq. (3) and (4), the droop gains ( $K_{I_i}^{dc}$ ,  $K_{P_i}^{dc}$ ) can be calculated based on the rated current and power of any  $DG_i^{dc}$ .

For the DC subgrid power flow, we define the current injection in an  $n$ -bus DC subgrid similarly to the AC subgrid, including an arbitrarily chosen virtual DC bus, as:

$$\begin{bmatrix} I_{vir}^{dc} \\ I_1^{dc} \\ \vdots \\ I_n^{dc} \end{bmatrix} = \begin{bmatrix} G_{(vir)(vir)} & G_{(vir)1} & \cdots & G_{(vir)n} \\ G_{1(vir)} & G_{11} & \cdots & G_{1n} \\ \vdots & \vdots & \ddots & \vdots \\ G_{n(vir)} & G_{n1} & \cdots & G_{nn} \end{bmatrix} \begin{bmatrix} V_{vir}^{dc} \\ V_1^{dc} \\ \vdots \\ V_n^{dc} \end{bmatrix} \quad (11)$$

$G$  in Eq. (11) represents the elements of the conductance matrix of the DC subgrid. We perform similar algebraic operations as mentioned for the AC subgrid to obtain the iterative power flow expression for the DC subgrid as:

$$(\mathbf{V}^{dc})^{k+1} = \mathbf{G}_B^{-1} (\mathbf{I}^{dc} - \mathbf{G}_A \cdot V_{vir}^{dc})^k \quad (12)$$

Unlike  $\mathbf{Y}_A$  and  $\mathbf{Y}_B$  in the AC subgrid,  $\mathbf{G}_A$  and  $\mathbf{G}_B$  in the DC subgrid do not need to be updated/calculated as they are not frequency-dependent. Therefore, in the DC subgrid power flow, only  $\mathbf{I}^{dc}$  and  $V_{vir}^{dc}$  need to be updated in every iteration. The calculation of the DC subgrid power flow is similar to that of the AC subgrid, as described previously, without frequency-related calculations.

### C. Power Flow in Interlinking Converter

The interlinking converter in an AC/DC hybrid microgrid facilitates active power exchange between the AC and DC subgrids based on the control strategy. A schematic representation of an interlinking converter connecting the AC subgrid at bus  $i$  and the DC subgrid at bus  $j$  is presented in Figure 1. The interlinking converter calculates the level of loading of the AC and the DC subgrid, and subsequently, it determines the power exchange  $P_{ic}$  between the two subgrids.

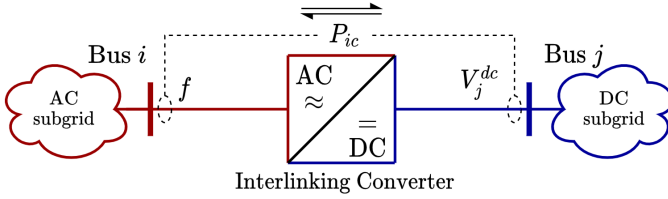


Fig. 1: Schematic representation of interlinking converter connecting the AC and DC subgrids.

The level of loading of the AC subgrid ( $f_{lol}$ ) and the DC subgrid ( $V_{lol_j}^{dc}$ ) is calculated as:

$$f_{lol} = \frac{f - 0.5(f_{max} + f_{min})}{0.5(f_{max} - f_{min})} \quad (13)$$

$$V_{lol_j}^{dc} = \frac{V_j^{dc} + 0.5(V_{max}^{dc} + V_{min}^{dc})}{0.5(V_{max}^{dc} - V_{min}^{dc})} \quad (14)$$

In Eq. (13) and (14),  $f_{max}$  is the maximum operating frequency of the AC subgrid,  $f_{min}$  is the minimum operating frequency of the AC subgrid,  $V_j^{dc}$  is the voltage of bus  $j$  of the DC subgrid,  $V_{max}^{dc}$  is the maximum operating voltage of the DC subgrid, and  $V_{min}^{dc}$  is the minimum operating voltage of the DC subgrid. The interlinking converter power  $P_{ic}$  is determined based on  $f_{lol}$  and  $V_{lol_j}^{dc}$  as:

$$P_{ic} = (f_{lol} - V_{lol_j}^{dc})/K_P^{ic} \quad (15)$$

In Eq. (15),  $K_P^{ic}$  is the droop gain of the interlinking converter. The interlinking converter transfers active power from the AC subgrid to the DC subgrid when  $(f_{lol} - V_{lol_j}^{dc}) > 0$ , while the reverse occurs when  $(f_{lol} - V_{lol_j}^{dc}) < 0$ . Transfer of active power between the two subgrids is essentially modeled as an active generation or load depending on the direction of power flow.

The power flow algorithm for the AC/DC hybrid microgrid is summarized in **Algorithm 1**.

---

#### Algorithm 1: AC/DC Hybrid Microgrid Power Flow

---

```

Set error tolerance;
Initialize AC/DC voltages, AC system frequency, and AC/DC
  specified droop gains;
Form conductance matrix of DC subgrid to obtain  $G_A$  and  $G_B$ ;
while error > error tolerance do
  Form/update admittance matrix of AC subgrid to obtain  $Y_A$  and
   $Y_B$ ;
  Calculate current injections  $I^{ac}$  and  $I^{dc}$ ;
  Calculate voltages  $V^{ac}$  and  $V^{dc}$ ;
  Calculate power injections through the virtual buses in AC and
  DC subgrids;
  Calculate AC subgrid frequency and corresponding DG
  injections;
  Calculate DG injections in DC subgrid;
  Equalize virtual bus voltages with their adjacent connecting
  buses in both AC and DC subgrids;
  Calculate interlinking converter power flow  $P_{ic}$  and allocate it as
  load and generation;
  Calculate voltage mismatch;
end
Output results;

```

---

### III. OPTIMIZATION PROBLEM FORMULATION

Optimal power flow is formulated as a constrained multi-objective nonlinear cost minimization problem. It is desirable

to operate a hybrid microgrid optimally to achieve better system states and lower operation cost. The objective function is, therefore, defined with the aim of minimizing the total generation cost of all the DGs in the hybrid microgrid whilst also minimizing the voltage deviations and the AC microgrid frequency deviation from their no-load values. The voltage and frequency deviation terms are included in the cost function such that the optimal solution is not towards the extreme limits of voltage and frequency, which can impact the stability of the network [9]. Consequently, the cost function for the optimal power flow problem is written as:

$$\min \left( w_1 \sum_{i \in \mathcal{G}_{ac}} C_{DG_i}^{ac}(P_{G_i}^{ac}) + w_2 \sum_{i \in \mathcal{G}_{dc}} C_{DG_i}^{dc}(P_{G_i}^{dc}) \right. \\ \left. + w_3 \sum_{i \in \mathcal{N}_{ac}} (V_0^{ac} - V_i^{ac})^2 + w_4 \sum_{i \in \mathcal{N}_{dc}} (V_0^{dc} - V_i^{dc})^2 + w_5 (f_0 - f)^2 \right) \quad (16)$$

In Eq. (16), the generation cost for both AC ( $C_{DG_i}^{ac}(P_{G_i}^{ac})$ ) and DC ( $C_{DG_i}^{dc}(P_{G_i}^{dc})$ ) DGs are considered to be quadratic [10]. The weights ( $w_1, w_2, w_3, w_4, w_5$ ) are considered appropriately to unify the unit of the cost function. The cost of generation in the microgrid is much larger than the cost of voltage and frequency deviation, therefore it is sufficient to consider the quantity of all weights to be equal to 1.

The cost above is subject to the following constraints:

$$(P_{G_i}^{ac} + P_{ic_i}) - P_{L_i}^{ac} = |V_i^{ac}| \sum_{k \in \mathcal{N}_{ac}} |V_k^{ac}| [G_{ik}^{ac}(f) \cos(\delta_i - \delta_k) \\ + B_{ik}^{ac}(f) \sin(\delta_i - \delta_k)] \quad \forall i \in \mathcal{N}_{ac} \quad (17)$$

$$Q_{G_i}^{ac} - Q_{L_i}^{ac} = |V_i^{ac}| \sum_{k \in \mathcal{N}_{ac}} |V_k^{ac}| [G_{ik}^{ac}(f) \sin(\delta_i - \delta_k) \\ - B_{ik}^{ac}(f) \cos(\delta_i - \delta_k)] \quad \forall i \in \mathcal{N}_{ac} \quad (18)$$

$$P_{G_i}^{dc} - (P_{L_i}^{dc} + P_{ic_i}) = V_i^{dc} \sum_{k \in \mathcal{N}_{dc}} G_{ik}^{dc} V_k^{dc} \quad \forall i \in \mathcal{N}_{dc} \quad (19)$$

$$f = f_0 - K_{P_i}^{ac} P_{G_i}^{ac} \quad \forall i \in \mathcal{G}_{ac} \quad (20)$$

$$(P_{G_i}^{ac})_{min} \leq P_{G_i}^{ac} \leq (P_{G_i}^{ac})_{max} \quad \forall i \in \mathcal{G}_{ac} \quad (21)$$

$$(Q_{G_i}^{ac})_{min} \leq Q_{G_i}^{ac} \leq (Q_{G_i}^{ac})_{max} \quad \forall i \in \mathcal{G}_{ac} \quad (22)$$

$$(P_{G_i}^{ac})^2 + (Q_{G_i}^{ac})^2 \leq (S_{G_i}^{ac})_{max}^2 \quad \forall i \in \mathcal{G}_{ac} \quad (23)$$

$$(P_{G_i}^{dc})_{min} \leq P_{G_i}^{dc} \leq (P_{G_i}^{dc})_{max} \quad \forall i \in \mathcal{G}_{dc} \quad (24)$$

$$(P_{ic_i})_{min} \leq P_{ic_i} \leq (P_{ic_i})_{max} \quad \forall i \in \mathcal{C}_{ic} \quad (25)$$

$$(|V_i^{ac}|)_{min} \leq |V_i^{ac}| \leq (|V_i^{ac}|)_{max} \quad \forall i \in \mathcal{N}_{ac} \quad (26)$$

$$(\delta_i)_{min} \leq \delta_i \leq (\delta_i)_{max} \quad \forall i \in \mathcal{N}_{ac} \quad (27)$$

$$(V_i^{dc})_{min} \leq V_i^{dc} \leq (V_i^{dc})_{max} \quad \forall i \in \mathcal{N}_{dc} \quad (28)$$

$$f_{min} \leq f \leq f_{max} \quad (29)$$

Constraint Eq. (17) and (18) represent the active and reactive power flow balance of the AC subgrid, while constraint Eq. (19) represents the power flow balance of the DC subgrid. Note that the admittance components  $G_{ik}^{ac}(f)$  and  $B_{ik}^{ac}(f)$  of the AC subgrid are frequency-dependent. Furthermore,  $G_{ik}^{ac}(f)$ ,  $B_{ik}^{ac}(f)$ ,  $G_{ik}^{dc}$  represent the admittance and conductance elements of the original respective subgrids without consideration of the virtual

TABLE I: Sets in the model

$\mathcal{N}_{ac}$	Set of AC buses
$\mathcal{N}_{dc}$	Set of DC buses
$\mathcal{G}_{ac}$	Set of DGs in the AC subgrid
$\mathcal{G}_{dc}$	Set of DGs in the DC subgrid
$\mathcal{C}_{ic}$	Set of Interlinking Converters

TABLE II: Parameters and Variables in the model

$P_{G_i}^{ac}$	Active power generation by $DG_i^{ac}$ at bus $i$ in the AC subgrid
$C_{DG_i}^{ac}(P_{G_i}^{ac})$	Cost of generation due to $DG_i^{ac}$ at bus $i$ in the AC subgrid
$P_{ic_i}$	Active power flow via interlinking converter $i$
$P_{L_i}^{ac}$	Active power load at bus $i$ in the AC subgrid
$ V_i^{ac} $	Voltage magnitude of bus $i$ in the AC subgrid
$\delta_i$	Voltage angle of bus $i$ in the AC subgrid
$G_{ik}^{ac}(f)$	Real part of the AC subgrid admittance element $(i, k)$ at frequency $f$
$B_{ik}^{ac}(f)$	Imaginary part of the AC subgrid admittance element $(i, k)$ at frequency $f$
$Q_{G_i}^{ac}$	Reactive power generation by $DG_i^{ac}$ at bus $i$ in the AC subgrid
$Q_{L_i}^{ac}$	Reactive power load at bus $i$ in the AC subgrid
$P_{G_i}^{dc}$	Active power generation by $DG_i^{dc}$ at bus $i$ in the DC subgrid
$C_{DG_i}^{dc}(P_{G_i}^{dc})$	Cost of generation due to $DG_i^{dc}$ at bus $i$ in the DC subgrid
$P_{L_i}^{dc}$	Active power load at bus $i$ in the DC subgrid
$V_i^{dc}$	Voltage magnitude of bus $i$ in the DC subgrid
$G_{ik}^{dc}$	Element $(i, k)$ of the DC subgrid conductance matrix
$f, f_0$	$f$ is the system frequency, $f_0$ is the no-load frequency
$K_{P_i}^{ac}$	Droop gain of $DG_i^{ac}$ at bus $i$ in the AC subgrid
$S_{G_i}^{ac}$	Apparent power generation by $DG_i^{ac}$ at bus $i$ in the AC subgrid

bus. Constraint Eq. (20) represents the voltage frequency, active droop gain, and power generation relationship of the DGs. The remaining constraint equations define the lower  $(\cdot)_{min}$  and upper  $(\cdot)_{max}$  limits of the parameters and variables.

The sets, parameters and variables related to the optimization problem are presented in Table I and II, respectively. The solution of the optimization problem yields optimal voltages (AC and DC), power injections (AC and DC), frequency, and active droop gains for the DGs in the AC subgrid. The optimal reactive droop gains for the DGs in the AC subgrid and the optimal active droop gains of the DGs in the DC subgrid are directly calculated based on Eqs. (2) and (10) from the optimal solution. Consequently, no additional constraints are required for reactive and active droop gains for the AC and DC DGs, respectively. Further details of the optimization problem should be referred to in [10].

#### IV. CASE STUDY

The 12-bus islanded AC/DC hybrid microgrid [3] presented in Figure 2 is used in this case study. The hybrid microgrid comprises a 6-bus AC subgrid and a 6-bus DC subgrid interconnected by a single interlinking converter. All DGs in the hybrid microgrid operate in droop controlled mode except the

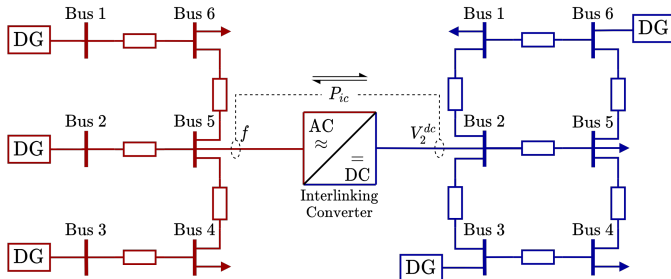


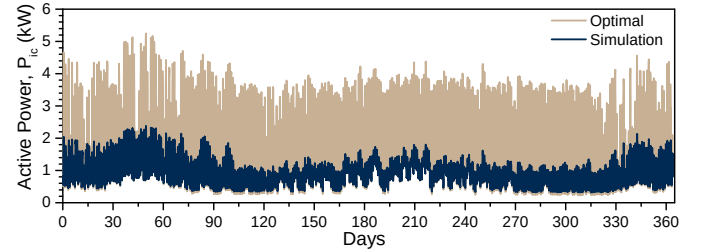
Fig. 2: 12-bus Islanded AC/DC Hybrid Microgrid.

DG connected at bus 2 of the AC subgrid. DG at bus 2 in the AC subgrid is assumed to be a solar PV plant of 10 kW peak capacity, which operates in PQ injection mode to maximize the renewable feed into the microgrid. Solar irradiance data for San Diego, California, USA, for the year 2019 at hourly resolution was collected [11] for simulation purposes. Similarly for the loads in the microgrid, a one-year load profile in hourly resolution was obtained from OpenDSS [12].

Two cases were investigated. The first one was year-long conventional operation of the hybrid microgrid with fixed droop gains, while the second one considered year-long optimal operation of the hybrid microgrid. The fixed droop gains for the conventional operation were calculated based on Eq. (3) and (4). Simulations were undertaken in a workstation having two Intel® Xeon® E5-2630V3 CPUs with 128GB of RAM. Both the simulation and optimization were performed in MATLAB®. The optimal power flow was formulated and solved utilizing the Optimization Toolbox in MATLAB® to obtain the optimal operation. Further details regarding the network simulation parameters should be referred to in [10].

#### V. RESULTS AND ANALYSIS

The power transfer through the interlinking converter throughout the year for both conventional and optimal operation is presented in Figure 3. In optimal operation of the microgrid,


 Fig. 3: Power through the interlinking converter ( $P_{ic}$ ).

higher power is transferred to the DC subgrid due to its higher loading and lesser generation as opposed to the conventional operation (having fixed droop gain of the interlinking converter). The hourly droop gain for the optimal operation is easily obtained from the optimal solution or the interlinking converter could also be operated to follow the fixed power transfer schedule of Figure 3.

Figure 4 presents the voltage profiles of all the DC buses for the month of January. Buses 4 and 5 are observed to violate the lower voltage limit several times under conventional operation as depicted. However, this is no longer observed under optimal operation of the grid, where sufficient power is transferred by the interlinking converter to improve the voltages in the DC subgrid and attain cost optimal operation.

Figure 5 presents the generation profiles of the DGs in the microgrid. It is observed in Figure 5(a) that under conventional operation, DGs at buses 1 and 3 in the AC subgrid start to consume power according to their fixed droop gains. This occurs when the solar PV generation by DG at bus 2 exceeds the load demand in the AC subgrid. As a result, the droop operation of the DGs start to consume power under  $P - f$

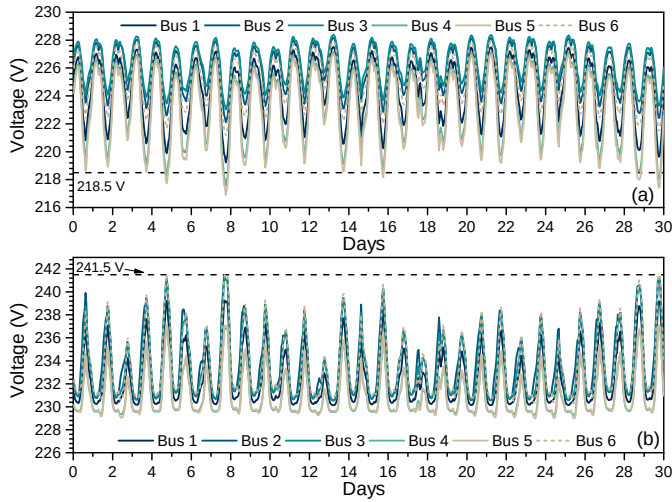


Fig. 4: Bus voltage (DC subgrid). (a) Conventional operation (b) Optimal operation.

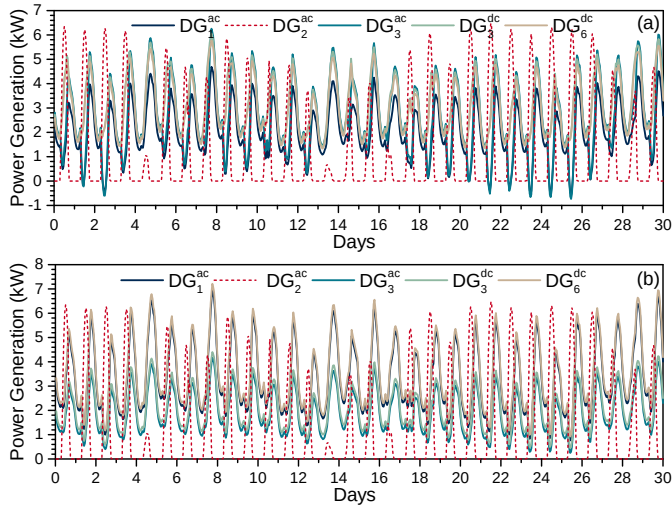


Fig. 5: Active power generation by all DGs. (a) Conventional operation (b) Optimal operation.

operation. In practice, such a scenario would encourage installation of battery storage or curtailment of DGs in the network. However, under optimal operation of the microgrid, this situation is effectively mitigated.

The optimal operation of the hybrid microgrid yielded annual losses of 331.2 kWh in the AC subgrid and 495.6 kWh in the DC subgrid, while the conventional operation yielded annual losses of 326.4 kWh in the AC subgrid and 512.6 kWh in the DC subgrid. The optimal operation yielded a cost saving of \$263 for the year's operation. This is significant for a hybrid microgrid of such a small size and, therefore, it is expected that the cost savings in larger interconnected hybrid microgrids will increase significantly under optimal operation. Some additional results can be referred to in [10].

In summary, the case study presented gives an understanding of the power flows in the hybrid microgrid by identifying important impacts of conventional operation. The case study also identifies the optimal operation of the hybrid microgrid

to mitigate adversities arising from conventional operation and quantifies the benefits of optimal operation like reduction in network losses, frequency and voltage deviations, and cost for a year-long operation.

## VI. CONCLUSION

This manuscript presented a single-phase implicit  $Z_{BUS}$  power flow approach combined with a multi-objective optimal power flow formulation for analysing islanded AC/DC hybrid microgrids. The year-long case study highlighted the benefits of incorporating the presented optimization problem into the operation of the hybrid microgrid. The results show a significant reduction in operation cost and power losses without exceeding system boundaries, compared to conventional operation. The presented multi-objective formulation is general and can be applied to study generic hybrid microgrids. In future research, ways to reduce the temporal effort of the optimization will be investigated along with the optimal operation of unbalanced hybrid microgrids.

## ACKNOWLEDGMENT

This work was financially supported by the Singapore National Research Foundation under its Campus for Research Excellence And Technological Enterprise (CREATE) programme.

## REFERENCES

- [1] S. K. Chaudhary, J. M. Guerrero, and R. Teodorescu, "Enhancing the capacity of the AC distribution system using DC interlinks—a step toward future DC grid," *IEEE Transactions on Smart Grid*, vol. 6, no. 4, pp. 1722–1729, 2015.
- [2] S. Salman and A. Xin, "Droop control based approach for frequency and voltage in hybrid AC/DC microgrid," *Journal of Electrical Engineering & Technology*, pp. 1–10, 2020.
- [3] E. E. Pompodakis, G. C. Karyonidis, C. S. Demoulias, and M. C. Alexiadis, "A generic power flow algorithm for unbalanced islanded hybrid AC/DC microgrids," *IEEE Transactions on Power Systems*, 2020.
- [4] M. A. Allam, A. A. Hamad, and M. Kazerani, "A sequence-component-based power-flow analysis for unbalanced droop-controlled hybrid AC/DC microgrids," *IEEE Transactions on Sustainable Energy*, vol. 10, no. 3, pp. 1248–1261, 2018.
- [5] A. Eajal, M. A. Abdelwahed, E. El-Saadany, and K. Ponnambalam, "A unified approach to the power flow analysis of AC/DC hybrid microgrids," *IEEE Trans. Sustain. Energy*, vol. 7, no. 3, pp. 1145–1158, 2016.
- [6] H. M. Ahmed, A. B. Eltantawy, and M. Salama, "A generalized approach to the load flow analysis of AC–DC hybrid distribution systems," *IEEE Transactions on Power Systems*, vol. 33, no. 2, pp. 2117–2127, 2017.
- [7] E. Pompodakis, A. Ahmed, and M. C. Alexiadis, "A three-phase weather-dependent power flow approach for 4-wire multi-grounded unbalanced microgrids with bare overhead conductors," *IEEE Transactions on Power Systems*, 2020.
- [8] M. A. Allam, A. A. Hamad, and M. Kazerani, "A generic modeling and power-flow analysis approach for isochronous and droop-controlled microgrids," *IEEE Transactions on Power Systems*, vol. 33, no. 5, pp. 5657–5670, 2018.
- [9] Z. Shuai, Y. Sun, Z. J. Shen, W. Tian, C. Tu, Y. Li, and X. Yin, "Microgrid stability: Classification and a review," *Renewable and Sustainable Energy Reviews*, vol. 58, pp. 167–179, 2016.
- [10] A. Ahmed, "Optimal operation of islanded AC/DC hybrid microgrids: Supplementary information," <https://github.com/arifa7med/PESGM2021/blob/main/supplementary.pdf>.
- [11] S. Pfenninger and I. Staffell, "Long-term patterns of European PV output using 30 years of validated hourly reanalysis and satellite data," *Energy*, vol. 114, pp. 1251–1265, 2016.
- [12] R. C. Dugan, "Reference guide: The open distribution system simulator (OpenDSS)," *Electric Power Research Institute, Inc.*, vol. 7, p. 29, 2012. [Online]. Available: <https://spinengenharia.com.br/wp-content/uploads/2019/01/OpenDSSManual.pdf>